Journal of Alloys and Compounds 509 (2011) 990–996

Contents lists available at ScienceDirect

Journal of Alloys and Compounds

journal homepage: www.elsevier.com/locate/jallcom

Pressureless sintering of internally synthesized SiC-TiB_2 composites with improved fracture strength

Dusan Bucevac[a,b,*], Branko Matovic[b], Snezana Boskovic[b], Slavica Zec[b], Vladimir Krstic[a]

[a] Department of Mechanical and Materials Engineering, Queen's University, Kingston, Ontario K7L 3N6, Canada
[b] Institute of Nuclear Sciences Vinca, University of Belgrade, P.O. Box 522, Belgrade 11001, Serbia

ARTICLE INFO

Article history:
Received 6 June 2010
Received in revised form
15 September 2010
Accepted 17 September 2010
Available online 20 October 2010

Keywords:
Silicon carbide
Ceramics
Sintering
Mechanical properties
Optical microscopy

ABSTRACT

SiC-TiB_2 particulate composites were fabricated by converting TiO_2 to TiB_2 through the reaction between TiO_2, B_4C and C. The presence of initially very fine, *in-situ* created, TiB_2 particles increased driving force for sintering and enabled fabrication of a dense composite utilizing pressureless sintering and the liquid phase created between Al_2O_3 and Y_2O_3 additives. The effect of volume fraction of the *in-situ* formed TiB_2 on density, microstructure and flexural strength was discussed. It was found that the presence of TiB_2 particles suppressed the growth of SiC grains and enhanced fracture strength. The fracture strength of samples containing 12 vol% TiB_2 was more than 30% higher than that of the monolithic SiC. The effect of SiC grain size on fracture strength was also analyzed.

1. Introduction

SiC possesses unique combination of thermo-mechanical properties which makes it one of the most suitable structural ceramics for both high- and low-temperature applications [1]. However, wider application of SiC as structural material is limited by relatively low fracture toughness and service reliability. The development of elongated SiC grain structure has been a powerful method of increasing fracture toughness of the sintered SiC [2,3]. The presence of elongated SiC grains was found to be beneficial for activation of toughening mechanisms such as crack bridging [4] and crack deflection [5]. Although the elongation of SiC grains is beneficial in raising fracture toughness, their presence increases the scatter in properties and leads to a decrease in fracture strength [6,7]. One of the methods of improving both the strength and fracture toughness of SiC is the reinforcement with particles having different elastic and thermal properties such as TiC [8] and TiB_2 [9]. It is believed that the difference in elastic, thermal and fracture properties between the reinforcements and SiC matrix serves to activate some of the toughening mechanisms typical for the particular composites. For example, higher thermal expansion coefficient of TiB_2 ($\alpha = 8.65 \times 10^{-6}\,^{\circ}C^{-1}$) [10], compared to that of SiC matrix ($\alpha = 4.75 \times 10^{-6}\,^{\circ}C^{-1}$) [11], creates a compressive residual thermoelastic stress around the TiB_2 particles during cooling from the fabrication temperature. This compressive stress interacts with the tensile stress at the crack tip resulting in a new relaxed crack tip stress filed and in an increase in fracture toughness of the composite [12]. In addition to toughening effect, the presence of reinforcing particles could also suppress growth of SiC grains which normally leads to improved strength [13].

So far, two different methods have been used to fabricate dense SiC-TiB_2 composites. One is the so-called solid state sintering with the addition of B and C [13] and the other is the liquid phase sintering in the presence of liquid forming additives such as Al_2O_3 and Y_2O_3 [10,14]. The major problem with the solid state sintering is that it requires very high sintering temperature (>2200 °C) which creates problems with exaggerated grain growth and evaporation of TiB_2 phase. Liquid phase sintering, on the other hand, requires much lower sintering temperature but the driving force for sintering is too low to give sufficiently high density without the use of hot pressing. For this reason hot pressing has been the preferential method of densification for SiC ceramics with externally added TiB_2 particles [10,14].

In this work, TiB_2 particles were created by the internal synthesis involving TiO_2, B_4C and carbon as raw materials. Newly created TiB_2 particles, which are initially very fine and active, provide additional driving force for sintering and allow fabrication of the composite with densities exceeding 98% of the theoretical

* Corresponding author at: Institute of Nuclear Sciences Vinca, University of Belgrade, P.O. Box 522, Belgrade 11001, Serbia.
Tel.: +381 11 340 8662; fax: +381 11 340 8224.
E-mail address: bucevac@vinca.rs (D. Bucevac).

0925-8388/$ – see front matter © 2010 Elsevier B.V. All rights reserved.
doi:10.1016/j.jallcom.2010.09.152

density (TD), without the need for hot pressing. The internal synthesis of TiB_2 is based on the following reaction which takes place at temperature lower than the sintering temperature [15]:

$$2TiO_2 + B_4C + 3C \rightarrow 2TiB_2 + 4CO \uparrow (\sim 1450\,^{\circ}C) \quad (1)$$

The present work describes the effect of the volume fraction of *in-situ* formed TiB_2 on density and strength of pressureless sintered SiC-TiB_2 composites. The sintering was performed at 1940 °C in the presence of Al_2O_3 and Y_2O_3 as liquid forming additives. The sintering temperature of 1940 °C was selected based on the results obtained in the previous study [16] which showed that 1940 °C is the temperature that provides highest density and fracture toughness of the composites.

2. Experimental

2.1. Sample preparation

Commercially available β-SiC (0.7 μm) (Functional Materials Manufacturing Inc.), Al_2O_3 powder (Alcoa A-16 SG, Bauxite, USA), high purity Y_2O_3 powder (Alpha Aesar), sub-micrometer TiO_2 powder (Fuji Titan Kogyo, anastase type), sub-micrometer B_4C powder (Electro Abrasive, USA) and high surface area graphite powder (Aldrich Chemical Company, Inc, USA) were used as starting materials. The amount of TiO_2, B_4C and C was adjusted so as to yield volume fractions of TiB_2 particles ranged from 6% to 50%. The amount of Al_2O_3 and Y_2O_3 sintering aids used in the present work was 4.3 wt% and 5.7 wt%, respectively. The initial powders and binder (5 wt% polyethylene-glycol) were mixed by ball milling in a plastic jar using ZrO_2 as milling media and methanol as a liquid vehicle. After milling for 12 h, the mix was dried at 90 °C followed by sieving and pressing into pellets (35 mm × 16 mm × 8 mm) under a pressure of 50 MPa. In order to increase the green density and make it uniform, all green compacts were isostatically pressed at a pressure of 250 MPa for 2 min. Before sintering, the green compacts were slowly heated to 650 °C in order to remove the organic binder. The sintering was done by first heating the samples to 1450 °C under vacuum (~5×10^{-2} torr) and holding at that temperature for 1 h in order to allow the conversion reaction to be completed. After 1 h, argon was introduced and the samples were heated to 1940 °C to complete the densification. The pressure in the furnace was adjusted to be equal to the atmospheric pressure. The samples were held at 1940 °C for 1 h before cooling to room temperature.

2.2. Characterization

The sintered samples were machined into rectangular bars with approximate dimensions 3 mm × 4 mm × ~27 mm. The density of the samples was measured using Archimedes' method. The relative density was calculated based on the theoretical density assuming a rule of mixture. Four-point flexural strength measurement was carried out on a tool steel jig with an inner span of 13.27 mm and the outer span of 23.88 mm. The samples used for hardness measurements were chosen from the broken pieces from the flexural strength test. Hardness was estimated by measuring diagonal length of the indent made by 5 kg load Vicker's indenter. The microstructures of polished, etched and fractured surfaces were observed by optical and scanning electron microscopies. The polished surfaces were electrochemically etched in KOH solution.

3. Results and discussion

3.1. Density and weight loss

The effect of volume fraction of TiB_2 on density and weight loss of sintered samples is presented in Fig. 1. The observed weight loss, which varies between 3% and 5%, is due to the evaporation of material through the reaction between SiC and the Al_2O_3 sintering aid [17]. As Fig. 1 shows, the weight loss of sintered samples decreases after the addition of up to 18 vol% TiB_2 and stays almost constant with further increase in volume fraction of TiB_2. The main reason for a decrease in weight loss of the samples containing TiB_2 is the reduced contact area between SiC and Al_2O_3 due to partial replacement of SiC with TiB_2 which in turn reduces the likelihood of the reaction between SiC and Al_2O_3.

As displayed in Fig. 1, the density increases with the volume fraction of TiB_2 reaching a maximum value for samples containing 18 vol% TiB_2. The increase in density indicates that the presence

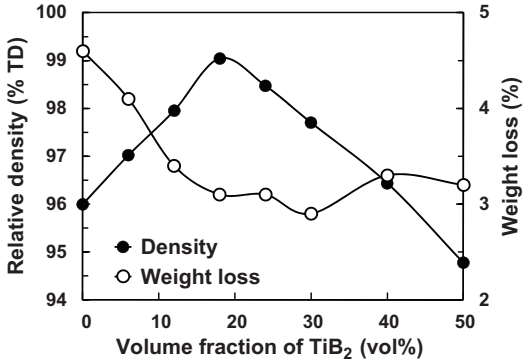

Fig. 1. Effect of volume fraction of TiB_2 on relative density and weight loss of sintered samples.

of extremely fine, *in-situ* created TiB_2 particles as well as suppression of weight loss is sufficient to improve the density of SiC-TiB_2 composites compared to that of a monolithic SiC. However, when the volume fraction of TiB_2 exceeds 18% the density of the composite starts to decrease. The decrease in density, despite almost constant weight loss, points out that the additional porosity, created due to the release of CO gas during $TiO_2 \rightarrow TiB_2$ conversion, is responsible for the decrease in density. It is worth noting that even samples with 30 vol% TiB_2 can be densified in excess of 97% TD. However, low density of the samples containing more than 30 vol% TiB_2 suggests that the high porosity created by the conversion reaction cannot be eliminated even though the fraction of fine, newly created TiB_2 particles is high. For example, the density of samples with 50 vol% TiB_2 immediately after conversion of TiO_2 to TiB_2 is only 32% TD whereas the green density of samples without TiB_2 is over 52% TD. The properties of samples with 50 vol% TiB_2 will not be discussed further as they will not be used for mechanical property testing.

3.2. Phase composition

The X-ray patterns of the samples with different volume fractions of TiB_2 are shown in Fig. 2. The figure shows that the structure consists of two major crystalline phases, SiC and TiB_2, and two minor crystalline phases, YAG ($3Y_2O_3{\cdot}5Al_2O_3$) and a 1:1 phase with the formula $Y_2O_3{\cdot}Al_2O_3$ [18]. The minor phases are the result of crystallization of the liquid phase created by Al_2O_3 and Y_2O_3 additives. The characteristic (strongest) peak of TiO_2, at approximately 48°, was not detected indicating that the content of residual TiO_2 was below detection limit (~1–3%). It is important to note that an increase in the volume fraction of TiB_2 is followed by the decrease in the amount of 1:1 phase. The formation of YAG phase is expected since the Y_2O_3/Al_2O_3 ratio in this compound is the same as the

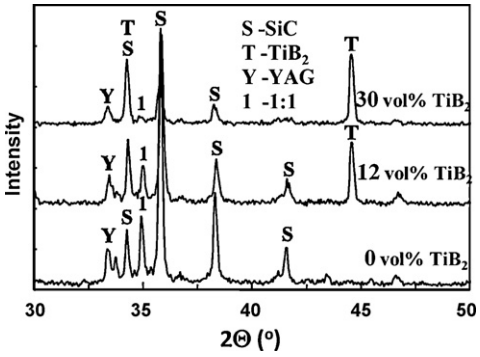

Fig. 2. X-ray patterns of sintered samples with different volume fractions of TiB_2.

Y_2O_3/Al_2O_3 ratio in the added mixture of Y_2O_3 and Al_2O_3 (57 wt% Y_2O_3/43 wt% Al_2O_3). The formation of 1:1 phase is considered to be due to the reaction between SiC and Al_2O_3 additive the result of which is highly volatile Al_2O. This reaction decreases the amount of Al_2O_3 in the liquid phase causing crystallization of 1:1 phase which contains lower fraction of Al_2O_3 (70 wt% Y_2O_3/30 wt% Al_2O_3) than the YAG phase. Large amount of 1:1 phase in the samples without TiB_2 (Fig. 2) is the result of intensive reaction between Al_2O_3 and SiC and the consequent lack of Al_2O_3 in the liquid phase.

3.3. Microstructure

Detailed microstructural examination reveals that the volume fraction of TiB_2 particles strongly influences the morphology of both the SiC matrix and TiB_2 grains. The increase in volume fraction of TiB_2 continuously decreases the size (length) of SiC grains. Grain size measurements in monolithic SiC revealed the presence of grains more than 35 μm in length (Fig. 3(a)) whereas no SiC grains longer than 10 μm were measured in sample with 40 vol% TiB_2 (Fig. 3(f)). Noticeable refinement of SiC grains is observed in samples containing above 6 vol% TiB_2. As Fig. 3(b) shows, very long SiC grains can be seen in samples with 6 vol% TiB_2. It is also noticed that as the volume fraction of TiB_2 particles increases their size also increases. Besides the change in particle size, the shape of TiB_2 particles also changes from predominantly equiaxed particles, in samples with 6 and 12 vol% TiB_2, to clustered elongated particles in samples with 40 vol% TiB_2. The pronounced clustering starts when the volume fraction of TiB_2 exceeds 24 vol%. For example, most of the dispersed particles, in samples containing 40 vol% TiB_2, are clusters of several grains interconnected with each other.

3.4. Fracture strength

It is well known that the strength of the non-cubic (anisotropic) structural ceramics such as SiC strongly depends on grain size, pore size, porosity and residual stress [19]. Therefore the change in density (porosity) and the change in SiC grain size (length) with volume fraction of TiB_2 particles, presented in Figs. 1 and 3, respectively, are expected to affect the strength of the composite as well. It has been suggested that both grains and pores in polycrystalline ceramics form inherent flaws extending into the surrounding matrix (Fig. 4) [19]. As the figure shows, the critical crack responsible for fracture ($2C$) consists of inherent cracks (in the form of annular flaws) (s) and $2R$ which is either the grain diameter or pore diameter. Besides the fact that the grain/pore diameter directly affects the strength by changing the critical crack size ($2C$), it is also responsible for an additional increase in stress concentration at the tip of the crack which, in turn, decreases strength.

In general, there are two concepts which incorporate the effect of grain size, pores and residual stress on strength of anisotropic ceramics. The first concept involves the effect of grain size (length) and residual stress on strength and the second one involves the effect of pore size and pore volume fraction on strength. The first

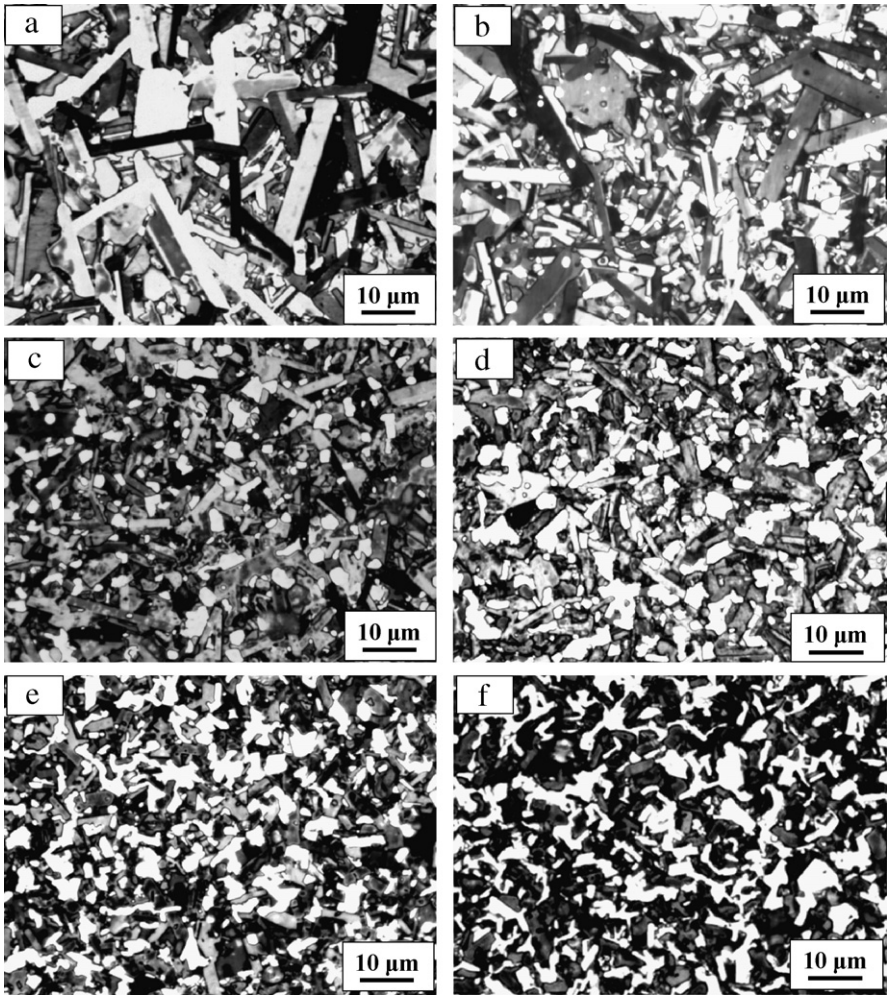

Fig. 3. Optical micrographs of etched surfaces of samples containing (a) 0 vol%, (b) 6 vol%, (c) 12 vol%, (d) 24 vol%, (e) 30 vol%, and (f) 40 vol% TiB_2. The white phase is TiB_2.

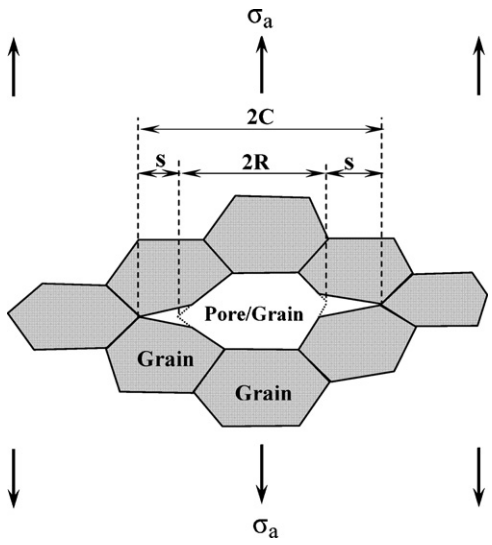

Fig. 4. Schematics of aggregate of grains in polycrystalline hexagonal ceramics showing annular flaws (s) emanating from the central grain/pore [19]. σ_a is the applied stress.

concept is presented by the following equation [20]:

$$\sigma_f = \left[\frac{\pi E \gamma_{eff}}{L(1+s/R)(1-\nu^2)}\right]^{1/2} - AP\Phi_t \quad (2)$$

where σ_f is the fracture strength, E is the Young's modulus, γ_{eff} is the effective fracture energy, L is the grain length, s is the annular flaw size, R is the grain half-length ($L=2R$), ν is the Poisson's ratio, A is a constant related to the level of residual stress relaxation, P is the residual thermoelastic stress and Φ_t is a constant expressed as:

$$\Phi_t = 1 - \left(1 - \frac{1}{(1+s/R)^2}\right)^{1/2} + \frac{1}{2(1+s/R)^{3/2}}\left(1 - \frac{1}{(1+s/R)^2}\right)^{1/2} \quad (3)$$

The residual stress P is given by the modified Selsing's equation [21]:

$$P = \frac{2E(\alpha_{\max} - \alpha_{\min})(T_{\max} - T_{\min})}{3(1-\nu)} = \frac{2E\,\Delta\alpha\,\Delta T}{3(1-\nu)} \quad (4)$$

where α_{max} is the linear thermal expansion coefficient in the direction of the highest thermal contraction (expansion), α_{min} is the linear thermal expansion coefficient in the direction of the lowest thermal contraction (expansion), T_{max} is the temperature from which the sample is cooled (1940 °C) and T_{min} is the temperature to which the sample is cooled (room temperature). The maximum anisotropic residual stress is expected to be generated when the central grain is oriented with the respect to the neighboring grains such that the axis of minimal thermal expansion (contraction) of the central grain is parallel to the axis of maximum thermal contraction of the surrounding grains. Under these conditions, the surrounding grains are subjected to the tensile stress which, in addition to the applied stress, causes the increase in the stress concentration at the crack tip and consequent decrease in strength. It is also worth noting that the annular flaw size (s) and grain half-length (R), given in Eq. (2), are not related to each other [19].

It is evident from Eq. (2) that the large value for grain length (L) is expected to reduce the strength of anisotropic material. Based on Eq. (2) it is clear that low fracture strength of samples with 0 and 6 vol% TiB_2, given in Fig. 5, is due to the presence of relatively

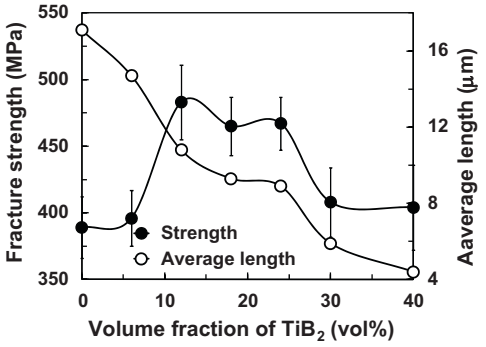

Fig. 5. Change of fracture strength and average length of elongated SiC grains with volume fraction of TiB_2.

long SiC grains known to reduce the strength of polycrystalline SiC [6,7]. As Fig. 5 shows, the average length of elongated SiC grains in samples containing no TiB_2 is ~17 μm. However, some of the SiC grains are as long as 85 μm and these grains actually determine the strength of the composite (see Fig. 6(a)). At approximately 12 vol% TiB_2, the average length of the SiC grains is reduced to ~10 μm at which point the strength reaches the highest value. For this composition, careful observation of polished surfaces revealed no grain longer than 50 μm.

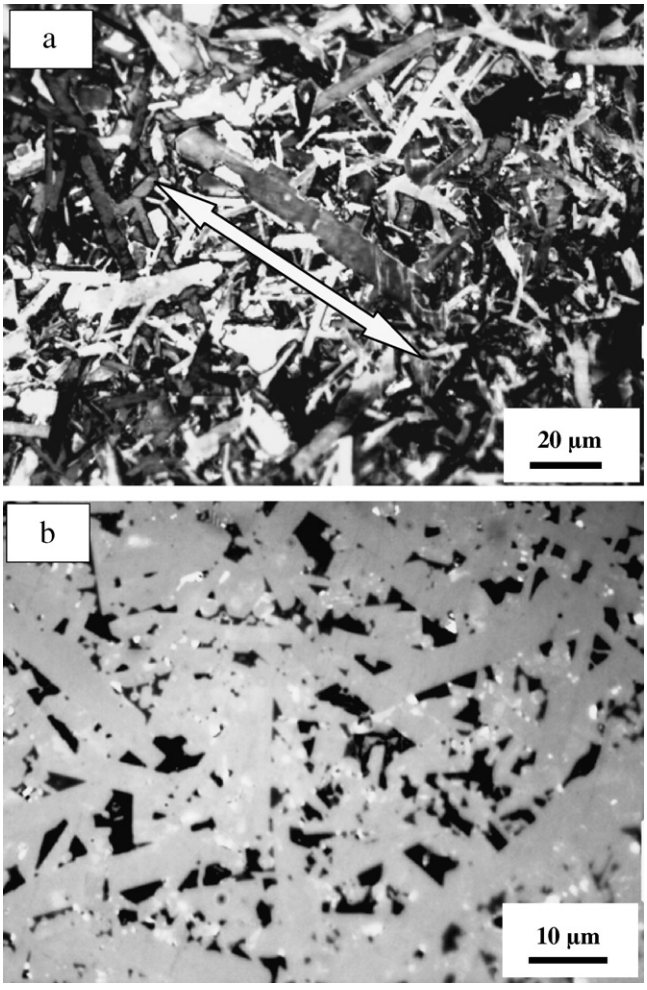

Fig. 6. Samples without TiB_2 (a) etched surface showing exaggerated SiC grain growth and (b) polished surface showing pore size. Magnification 400× and 1000×, respectively.

One can also argue that the higher strength of samples containing 12 vol% TiB_2 compared to that of monolithic SiC is also the result of higher density of the samples with 12 vol% TiB_2 (Fig. 1). Although it is well known that density (porosity) strongly affects strength, it is reasonable to assume that in compositions in which the length of SiC grains is much larger than the pore size, the effect of SiC grain length on strength is more pronounced than the effect of porosity. As Fig. 6(b) shows, there is large number of pores in samples without TiB_2 but the pore size is below 20 μm which is much smaller than the length of big SiC grains of ~85 μm.

Above approximately 12 vol% TiB_2, the relationship between strength and SiC grain length is opposite. As Fig. 5 shows, an increase in the volume fraction of TiB_2 above 12 vol% causes a decrease in the SiC grain length which is followed by a decrease in the fracture strength of the composite. Considerable decrease in strength was observed in samples containing above 24 vol% TiB_2. The observed decrease in strength with a decrease in SiC grain length cannot be explained by Eq. (2) as it clearly shows that the decrease in SiC grain length (L) is expected to increase strength. This implies that the strength of samples with more than 12 vol% TiB_2 is not controlled by the SiC grain length.

In order to further examine the relationship between the fracture strength and SiC grain length in samples containing 0–30 vol% TiB_2, the change of strength (from Eq. (2)) with SiC grain length (L) for various s/R values is presented in Fig. 7. Samples with 40 and 50 vol% TiB_2 are not discussed as their density was below 97% TD which is considered too low for structural applications. The effective fracture energy (γ_{eff}) of 30 J/m^2, Young's modulus of 415 GPa and Poisson's ratio of 0.17 [10] were used for calculation. The residual stress P was estimated through Eq. (4) using values for linear thermal expansion coefficients of SiC, $\alpha_{max} = 4.9 \times 10^{-6}\,^{\circ}C^{-1}$, $\alpha_{min} = 4.6 \times 10^{-6}\,^{\circ}C^{-1}$ [11] and $\Delta T = 1900\,^{\circ}C$. It was assumed that complete relaxation of anisotropic stress occurs during cooling from sintering temperature all the way to ~800 °C and the stress build up starts below 800 °C. On that basis, the value for constant A was selected to be ~0.42. The constant Φ_t was calculated through Eq. (3). In this calculation, the presence of TiB_2 particles was assumed to have only minor effect on the anisotropic behavior of the SiC matrix.

Fig. 7 shows that the decrease in SiC grain length is followed by the increase in fracture strength for all s/R values. Good fit between predicted and measured values is found for samples containing up to 12 vol% TiB_2. Based on Eq. (2), it is predicted that s/R ratio ranges from 1.4 in samples without TiB_2 to 1.8 in samples with 12 vol% TiB_2. It is also predicted from Eq. (2) that the annular flaw size is reduced from ~60 μm in samples with 0 and 6 vol% TiB_2 to ~45 μm in samples with 12 vol% TiB_2. This decrease in flaw size indicates

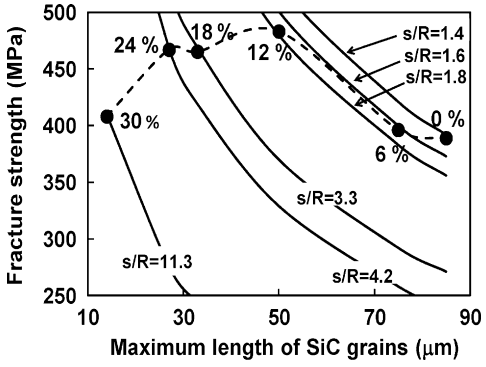

Fig. 7. Change of predicted values of fracture strength (solid lines) with SiC grain length for various s/R values (from Eq. (2)) and measured values for strength (designated as ●) of samples containing 0–30 vol% TiB_2.

that not only does the presence of 12 vol% TiB_2 decrease the SiC grain length but also it reduces the flaw size (s).

The decrease in strength of samples with more than 12 vol% TiB_2 despite further decrease in SiC grain length can be explained by the increase in the inherent flaw size (s). From Fig. 7 one can see that samples with 30 vol% TiB_2 have relatively large inherent flaw size of ~80 μm and s/R ratio of 11.3. However, the detail microstructural analysis reveals that it is more plausible that the big pores are the origin of fracture in samples containing more than 12 vol% TiB_2 rather than the elongated SiC grains with large emanating flaws. As Fig. 8(a) and (b) shows, the largest pore diameter in samples with 12 vol% and 24 vol% TiB_2 is 40 μm, approximately. These big pores are considered to be the origin of fracture in samples with 24 vol% TiB_2 since their diameter is larger than the SiC grain length which does not exceed 30 μm. In samples with 12 vol% TiB_2 it was much more difficult to determine the origin of fracture as the length of the longest SiC grain (~50 μm) was close to the size of the largest pore. Very small variation of strength of samples containing 12–24 vol% TiB_2 (~18 MPa), indicates that the cause of fracture in these compositions is the same, i.e., the presence of big pores. As the volume fraction of TiB_2 increases the size of the large pores also increases and for samples with 30 vol% TiB_2 it reaches the level of ~60 μm (Fig. 8(c)). The increase in pore size is believed to be the main reason for sharp drop in strength of these samples (Fig. 5).

The effect of porosity on fracture strength can be explained on the basis of the following equation [19]:

$$\sigma_f = \left[\frac{\pi\gamma_{eff}E_o}{D(1+s/r)(1-\nu^2)}\right]^{1/2}\left[1+\frac{4V_p(1-\nu^2)(1+s/r)^3}{\pi}\right]^{-1/2} \quad (5)$$

which relates the pore volume fraction, V_p, the pore diameter, D, and the inherent flaw size, s. Other parameters in Eq. (5) are the effective fracture energy, γ_{eff}, the Young's modulus of the pore free material, E_o, the pore radius, r, and the Poisson's ratio, ν.

Eq. (5) shows that an increase in pore volume fraction (V_p) is expected to reduce the fracture strength. The support to this is found in Fig. 9 which depicts both calculated values for strength as a function of pore volume fraction for various s/R values and the measured strength of samples containing 18–40 vol% TiB_2. As the figure shows there is the decrease in measured strength as pore volume fraction is increased (see Fig. 9). It can also be seen that the s/R ratio decreases continuously as the volume fraction of TiB_2 increases, which is believed to be the result of SiC grains refinement.

In conclusion, the presence of TiB_2 particles in SiC matrix plays an important role in inhibiting growth of SiC grains resulting in an increase in strength of the composite. While grain refinement is beneficial in enhancing the strength it limits the grain pull-out and excludes the possible crack bridging mechanism for toughening known to operate in SiC ceramics. The role of elongated SiC grains in strengthening of the composite is discussed in the next section.

3.5. Fracture surface

The nature of crack propagation in monolithic SiC and SiC with 24 vol% TiB_2 is revealed in Fig. 10 which shows SEM micrographs of the fracture surfaces. The examination of Fig. 10 reveals no signs of crack bridging which is one of the frequently observed mechanisms of strengthening and toughening in SiC. As can be seen in Fig. 10(a), a number of long SiC plates (>20 μm) in monolithic SiC fracture trans-granularly.

Contrary to what was expected, the less elongated SiC grains as well as equiaxed TiB_2 grains in the samples containing 24 vol% TiB_2 (Fig. 10(b)) appear to participate in crack deflection much

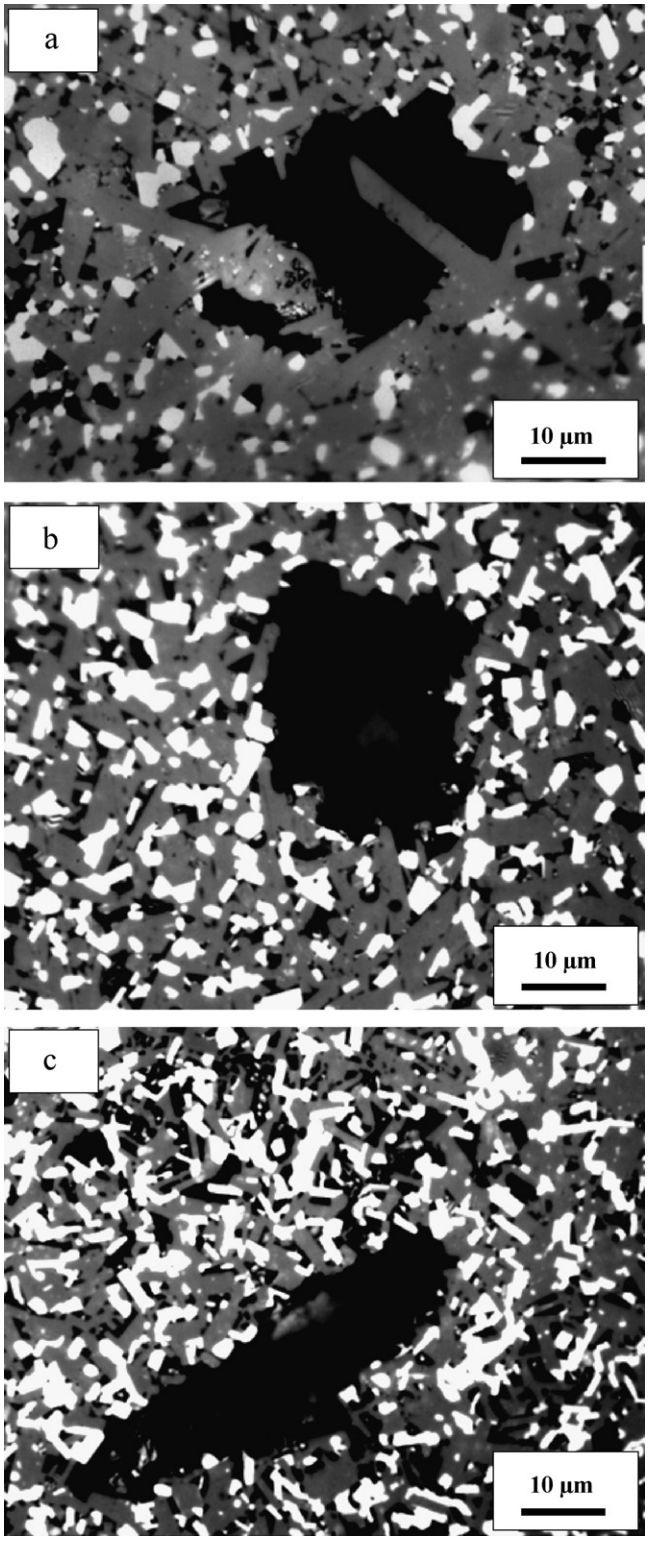

Fig. 8. Optical micrographs of polished surfaces showing porosity (black areas) in samples containing (a) 12 vol%, (b) 24 vol% and (c) 30 vol% TiB_2 (white areas).

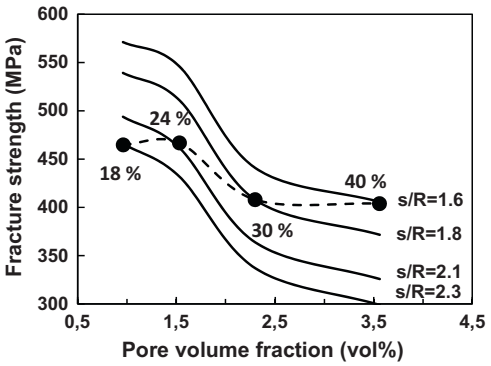

Fig. 9. Change of predicted values of fracture strength (solid lines) with pore volume fraction for various s/R values and the measured values for strength (designated as ●) of samples containing 18–40 vol% TiB_2. Predicted values for strength were determined by substituting appropriate values for $\gamma_{eff} = 30\,J/m^2$, $E_o = 420–435\,GPa$, and $D = 40\,\mu m$ (samples with 18 and 24 vol% TiB_2), $D = 60\,\mu m$ (samples with 30 and 40 vol% TiB_2) in Eq. (5).

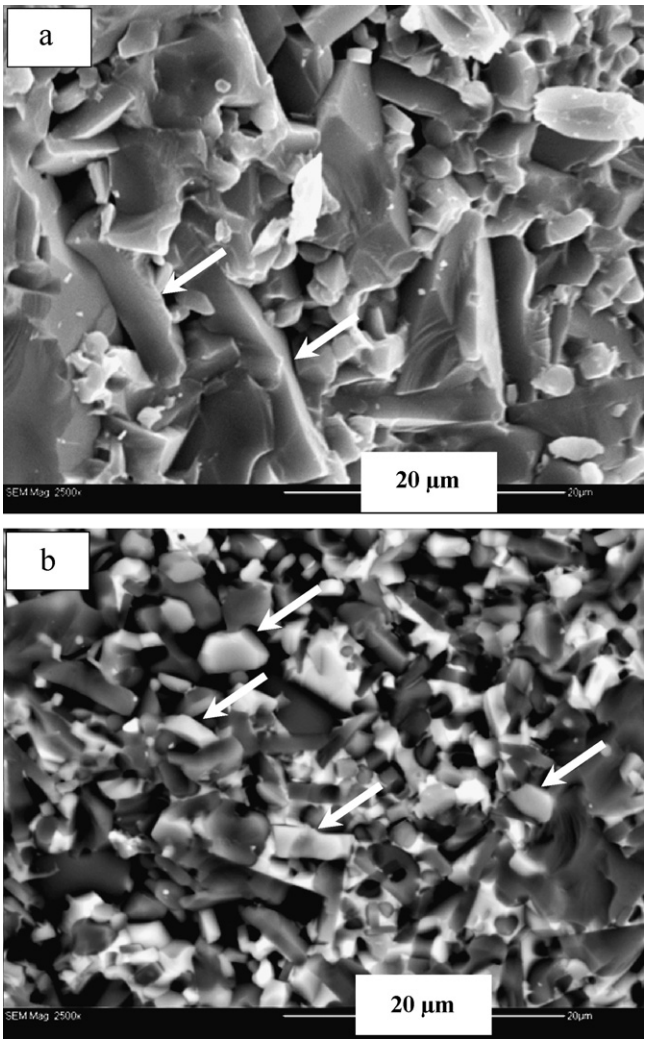

Fig. 10. SEM micrographs of fracture surfaces of samples with (a) 0 vol% TiB_2 (secondary electrons) showing trans-granular fracture of long SiC plates (arrows) and (b) 24 vol% TiB_2 (back scattering electrons) showing crack deflection (the arrows indicate TiB_2 particles).

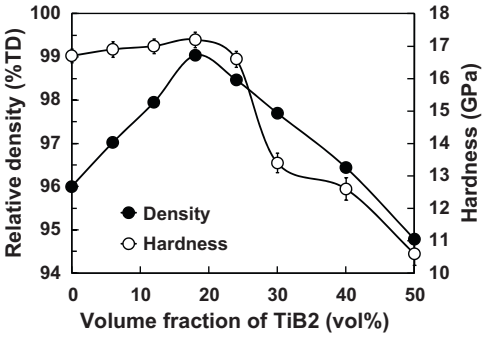

Fig. 11. Change of hardness and density of sintered samples containing different volume fractions of TiB_2.

more than elongated ones. The contribution of TiB_2 particles to toughening by crack deflection played an important role in improving the strength of samples containing TiB_2 especially those with 12–24 vol% TiB_2.

3.6. Hardness

The effect of volume fraction of TiB_2 on hardness is shown in Fig. 11. Despite the lower inherent hardness of TiB_2 compared to that of SiC, the graph in Fig. 11 shows that hardness of samples containing up to 18 vol% TiB_2 slightly increases as the volume fraction of TiB_2 increases. It appears that in this region the hardness is controlled entirely by the density of the sintered samples. Once the volume fraction of TiB_2 particles exceeds 18 vol% the hardness starts to decrease following the increase in porosity.

4. Conclusions

The internal synthesis of TiB_2 utilizing TiO_2, B_4C and C was found to be an effective way of producing dense SiC-TiB_2 composites with high strength. The presence of very fine, *in-situ* formed, TiB_2 particles has two beneficial effects. One is the increase in density of the composite due to both the high specific surface of newly created TiB_2 particles and suppressed reaction between SiC and Al_2O_3. The other effect is the inhibition of growth of SiC grains. The highest strength of 485 MPa was measured in samples containing 12 vol% TiB_2. The reduction in strength of samples containing above 24 vol% TiB_2 is attributed to an increase in pore size. Despite the lower inherent hardness of TiB_2, even the samples with 24 vol% TiB_2 have hardness close to that of monolithic SiC.

Acknowledgements

This work has been supported by the Ministry of Economic Development and Trade of Ontario and the Ministry of Science and Technological Development of the Republic of Serbia.

References

[1] A.W. Weimer, Carbide, Nitride and Boride Materials Synthesis and Processing, first ed., Chapman & Hall, London, 1997.
[2] S.G. Lee, Y.W. Kim, M. Mitomo, J. Am. Ceram. Soc. 84 (6) (2001) 1347–1353.
[3] S. Deshpande, T. Bhatia, H. Xu, N. Padture, A. Ortiz, F. Cumbrera, J. Am. Ceram. Soc. 84 (7) (2001) 1585–1590.
[4] M.A. Mulla, V.D. Krstic, Acta Metall. Mater. 42 (1) (1994) 303–308.
[5] K.T. Faber, A.G. Evans, Acta Metall. 31 (4) (1983) 565–576.
[6] J.Y. Kim, J.W. Kim, J.G. Lee, K.S. Cho, J. Mater. Sci. 34 (1999) 2325–2330.
[7] Y. Kim, M. Mitomo, H. Emoto, J. Lee, J. Am. Ceram. Soc. 81 (12) (1998) 3136–3140.
[8] G.C. Wei, P.F. Becher, J. Am. Ceram. Soc. 67 (8) (1984) 571–574.
[9] C.H. McMurty, W.D. Boecker, S.G. Seshadri, J.S. Zanghi, J. Garnier, Am. Ceram. Soc. Bull. 66 (2) (1987) 325–329.
[10] K.S. Cho, Y.W. Kim, H.J. Choi, J.G. Lee, J. Mater. Sci. 31 (1996) 6223–6228.
[11] Z. Li, R.C. Bradt, J. Am. Ceram. Soc. 69 (12) (1986) 863–866.
[12] A.K. Khaund, V.D. Krstic, P.S. Nicholson, J. Mater. Sci. 12 (1977) 2269–2273.
[13] J.D. Yoon, S.G. Kang, J. Mater. Sci. Lett. 14 (1995) 1065–1067.
[14] K.S. Cho, H.J. Choi, J.G. Lee, Y.W. Kim, J. Mater. Sci. 33 (1998) 211–214.
[15] M. Vlajic, V. Krstic, Process for the production of dense boron carbide and transition metal carbide, United States Patent No. 5,720,910, 1998.
[16] D. Bucevac, S. Boskovic, B. Matovic, V. Krstic, Ceram. Int. 36 (2010) 2181–2188.
[17] M.A. Mulla, V.D. Krstic, Ceram. Bull. 70 (1991) 439–443.
[18] J.S. Abell, I.R. Harris, J. Mater. Sci. 9 (1974) 527–537.
[19] V.D. Krstic, Theor. Appl. Fract. Mech. 45 (2006) 212–226.
[20] V.D. Krstic, M.D. Vlajic, Acta Metall. 31 (1983) 139–144.
[21] J. Selsing, J. Am. Ceram. Soc. 44 (1961) 419–420.